11

Egypt. J. Chem. **Vol. 65,** No. 1, pp. 99 - 106 (2022)

Egyptian Journal of Chemistry

http://ejchem.journals.ekb.eg/

Characterization of Atmospheric-Pressure DC-Glow Discharge in Contact with Liquid with a Miniature Argon Flow

Ahmed abdelradi [a,c]*, A. Samir [a], F. Elakshar [b], A. Garamoon [b], Mansour ElSabbagh [a,b]

[a]Center of Plasma Technology, Al-Azhar University-Cairo, Egypt

[b]Faculty of Science, Al-Azhar University, Cairo, Egypt

[c]Egyptian Meteorological Authority, Cairo, Egypt

Abstract

Atmospheric pressure dc glow discharges in contact with liquid with a miniature argon flow were created between a needle cathode and an electrolyte anode (NaCl solution) in the open air. The effect of argon flow in stabilizing the obtained discharge was explored. Electric characterization of the discharge was studied for electrode separation range from 1 to 12 mm at atmospheric pressure. The electrical characterization of the discharge revealed that the obtained Paschen curve showed a bi-straight line for the relation between the gas breakdown voltage and the product of the gas pressure p with the electrode separation distance d. The current-voltage characteristics of the discharge revealed that the discharge was operated in the normal glow mode. Optical characterization of the discharge showed that the discharge was strongly non-equilibrium, which is suitable for electrochemistry applications such as synthesizing magnetic nanoparticles from the iron electrode. Proposed chemical reaction routes for different electrochemical applications of DC glow discharge in contact with the liquid electrode were discussed.

Keywords: Electrochemistry; Spectroscopy; Plasma Chemistry; Glow Discharge; Pin-to-Liquid Discharge

1. Introduction

Electrochemical reactions generally proceed between an electronic rod and an ionic rod, with electrical charge moving crossways the boundary between these two phases. Although most electrochemical reactions are held out using liquid electrolytes such as aqueous solutions, non-aqueous solutions, or melted salts. A plasma is an ionized gas having equal numbers of positive and negative charges and usually a different number of non-ionized neutral molecules. One of the main types of stable plasmas is glow-discharge plasma (low-temperature plasma or non-equilibrium plasma). Atmospheric plasma DC glow discharge in contact with liquid is one of the simplest methods of obtaining a stable gas discharge plasma. Atmospheric non-thermal plasma in and in contact with liquids has been studied extensively for various applications in biomedical, nanomaterials synthesis, environmental and chemical engineering, as well as for general science issues in atmospheric chemistry and other scientific and engineering fields

[1–13]. Non-thermal plasmas (also known as non-equilibrium plasmas or cold plasmas) are typically characterized by their electron temperature (T_e), vibrational temperature (T_{vib}), rotational temperature (T_{rot}), and translational temperature (T_{trans}). In non-thermal plasmas created by externally applied electric fields typically $T_e > T_{vib} > T_{rot} = T_{trans}$ [14]. This paper investigated the characteristics of an atmospheric DC glow discharge using a liquid electrode with a miniature argon flow. The discharge system is considered an electrolytic system using plasma. Specifically, plasma acts as an electrode in electrolysis. The plasma electrode delivers electrons or ions into the liquid, creating reactions. When metal cations are melted in a solution, metallic nanoparticles are synthesized at the liquid by electron or positive ion irradiation from the plasma. One characterization technique is optical emission spectroscopy (OES), which can give information on the presence of various species in the discharge. We focus our attention on liquid reactions and chemical processes present during

the run, which is the main role for plasma liquid interaction application.

This paper is organized as follows. After this general introduction, Section 2 describes the experimental setup used for creating and analysing the discharge in contact with liquid. Section 3 presents the results of our work and the used characterization techniques; this section is divided into two parts; the first part is the electrical characterization. The second part is the spectroscopic characterization techniques for identifying emitting species and determining vibrational temperature (T_{vib}) and rotational temperature (T_{rot}).   While section 4 describes our discussions for chemical processes that occur in plasma liquid interaction. Finally, Section 5 presents our conclusions.

2. Experimental Setup

Figure 1 shows the schematic diagram for the experimental setup used for creating the discharge in contact with liquid and for the diagnostic techniques used to study the electrical and optical characterization of the discharge.   We used a nozzle cathode made of stainless-steel needle with an inner diameter of 500 µm and an outer diameter of 1mm. Working gas was argon, which was fed through the nozzle cathode, which was placed with varying gap distances above the surface of the electrolytic anode filled in a glass beaker as shown in figure (2). The gas flow rate was adjusted using a commercial flow meter to a value of 0.20 L/min in the whole work. A NaCl aqueous solution, with a 5 mg/ litre concentration, worked as the electrolytic anode. The discharge was powered by a regulated home-made dc power supply which can deliver applied voltage up to 10 kV. A ballast resistor of 100 kΩ was connected in series to the electrolytic anode. This ballast resistor is crucial to limit the discharge current in order to avoid the transition of the discharge to the arc mode. The electrolytic anode was connected to the ballast resistor through an iron spiral wire of 1 mm diameter and a length of 5 cm. The needle cathode was connected to the ground via a 100Ω resistor. The discharge current was measured by recording the voltage drop across the terminal of the 100Ω resistor. The gap voltage was measured using a home-made high-voltage probe. The voltage and current waveforms were recorded using (GDS-1000-U Series) digital storage oscilloscopes. The optical emission spectroscopy (OES) measurement in the discharge region centre was performed using Ocean

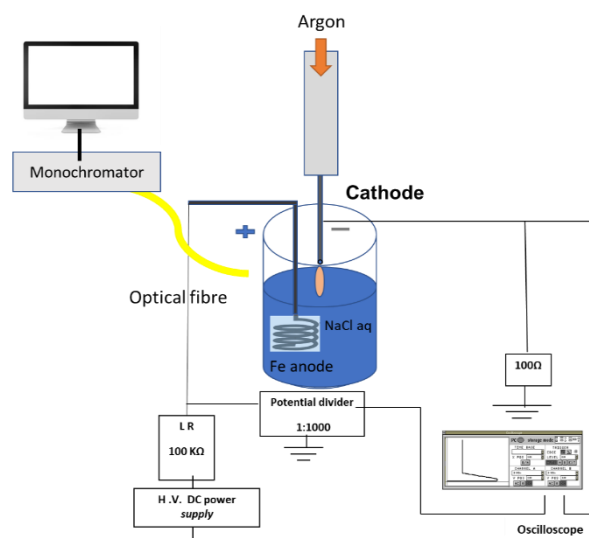optics' USB4000 dual fibre optic emission spectrometer.

Figure 1: Electric circuit used to generate and to analyze Stabilized glow discharge

Figure 2: Photograph of glow discharge in contact with liquid

3. Results and Discussion

3.1. Effect of Argon Flow on the Stability of the Generated Glow Discharge

It is well known that the generation of glow discharge at atmospheric pressure is not easy because of the discharge transition from the glow mode to arc or spark mode. The main reason for the transition of the glow to arc at atmospheric pressure is thermal instability. In literature, there are many techniques to generate stable atmospheric pressure glow discharge by avoiding the thermal instability by limiting the discharge current by using a suitable limiting resistance or electronically using a choke coil. Other techniques used to stabilize atmospheric pressure glow discharge are dissipating the thermal energy generated in the discharge by using massive electrodes or by using a flow of gas with high specific heat capacity.

In the current work, a miniature argon flow is used to stabilize the discharge. The use of a miniature argon flow effectively generates stable atmospheric discharges in the air. The argon flow generates a

streamlined flow from the needle cathode in ambient air. The discharge is generated along the streamline because the breakdown voltage in argon is much lower than that in air. In other words, the miniature argon flow constricts the discharge zone [15]. Figure 2 shows typical images of atmospheric DC glow discharges using the liquid anode with and without a miniature argon flow. With a miniature argon flow, both the discharge and the liquid surface appear static and stable as shown in figure 2. If the argon flow rate is too high, the liquid surface becomes turbulent. However, if a moderate streamline flow is generated, a stable discharge is realized even in a relatively long gap of several tens of millimeters.

The discharges are very unstable without an argon flow when the discharge current is lower than 11 mA. A conical discharge-shape is formed with increasing discharge current above 11 mA; nevertheless, it is less stable than the discharge with a miniature argon flow. Using a miniature argon flow, a glow discharge is generated with a stable plasma–liquid interface. Consequently, we examined atmospheric DC glow discharge characteristics using the liquid anode with a miniature argon flow to investigate the plasma–liquid interface for synthesizing magnetic nanoparticles.

3.2. Electrical Characterization

The chemical and physical processes occurrences at the plasma in contact with liquid are particularly composite; indefinitely glow discharge electrolysis has been used as a chemical tool. Attempts have been made to comprehend the chemistry and physics of these systems. There have been studies looking to characterize critical plasma parameters; one of these is electrical characteristics. In the current work, DC discharge was run to raise the applied voltage from the home-made DC power supply from zero volts. When argon gas breakdown was initiated through a rise in the applied voltage of the DC power supply, the voltage across the electrodes showed a sudden drop, and at the same time, a discharge current of a particular value was continuously flowing in the discharge circuit, as shown in figure 3. Figure 3 shows the current and voltage oscillograms for the electrolytic anode and needle cathode with a separation distance of 1mm and an argon flow rate of 0.2 litre per minute. The discharge current was 11mA and became constant with an increase in the applied voltage. The continuous form of the current-voltage waveform was observed in this investigation with all varying gap distances, which

indicates that the discharge was operated in continuous mode where there was no pulsed mode observed.
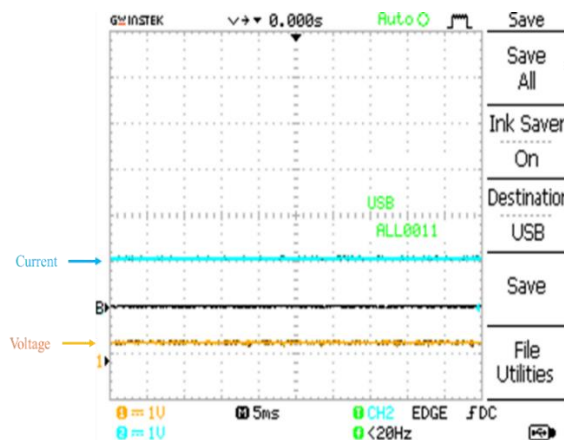

Figure 3: Current and voltage oscillograms for electrode separation of 1mm and argon flow rate of 0.2 liter per minute

3.2.1. Breakdown characteristics

The minimum required voltage to create a plasma between two electrodes is called the breakdown voltage V_{br}, which mainly depends on the type of gas, the gas pressure, and the gap size. Paschen's law was introduced in 1889 and stated that the breakdown voltage is a function of the product of the gap length d and gas pressure p ($V_{br}=f(pd)$)[16]. In the current work, the breakdown voltage was investigated for our discharge system, and to our knowledge, this is the first study of the Paschen curve, which shows the relation between the breakdown voltage and the product of the electrode separation times the gas pressure, for plasma generated between needle cathode and liquid anode.

The dependence of the breakdown voltage on the pd for the electrolytic anode and the needle cathode is depicted in figure 4. The data shown in figure 4 was obtained by changing the separation distance between the electrolytic electrode and the needle cathode from 1mm. up to 12 mm. while the argon pressure was kept constant at the atmospheric pressure. The pd at the minimum breakdown voltage in argon is about 1 Torr.cm [17]. This corresponds to an electrode space of 15 μm at atmospheric pressure. In the current work, the smallest spacing reliably achievable was 1mm, therefore, the data shown in figure 4 was a part of the right-hand side of the Paschen curve, and in addition, the Paschen minimum was not measured. For non-uniform electric field between electrodes and for higher pd than the Paschen minimum, the breakdown voltage was a logarithmic function of electrode spacing at a constant pressure of 760 Torr for air discharge with cathode plate and anode wire [18]. Meanwhile, the breakdown voltage against pd was a straight line for argon discharge in coaxial cylindrical

electrodes configuration [17]. The data shown in figure 4 revealed that the breakdown voltage of the right-hand side of the Paschen curve was not a logarithmic function of d at a constant pressure of 760 Torr. Instead, it was fitted by two straight lines with two different slopes. The first line has a smaller slope of 2.1V/Torr.cm, while the second line has a more significant slope of 9.2 V/Torr.cm. From figure 4, it is clearly seen that the slope of the line is changed for the data with d greater than 7 mm. (where p is kept constant at 760 Tor). The reason for obtaining bi-straight lines for breakdown voltage against pd is unclear, and more study is needed to explain it. To our knowledge, the bi-straight line behavior of breakdown voltage against pd was not observed in the literature before for both uniform and non-uniform electric field distribution between the discharge electrode
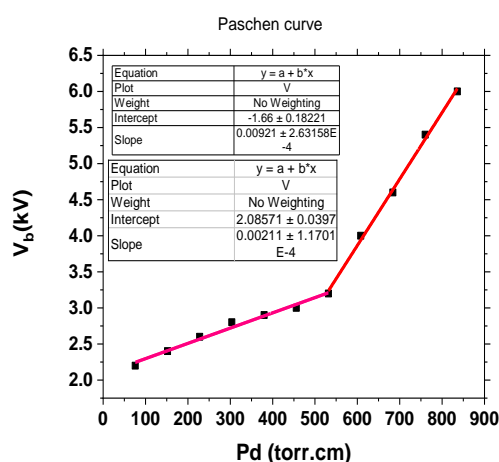

Figure 4: The dependence of the breakdown voltage on the pd parameter

3.2.2. Current-voltage characteristics

Current-voltage measurements are described in figure 5 for the discharge in contact with liquid, for electrode gap range of 1 to 12 mm. The measurements were recorded by the digital storage oscilloscopes. For the small spacing of electrodes, the $I-V$ characteristic is relatively consistent form. This is consistent with a normal glow discharge and previous measurements in atmospheric pressure glow discharge [19-21]. The discharge voltage upstairs occurs significantly in the positive column. The I-V characteristics have a negative dV/dI and a negative resistance for the more significant electrode gap. This might be due to the neutral gas temperature gradient through the positive column. It is clearly seen from figure 5 that, for a fixed separation electrode distance d, the discharge voltage required to sustain the discharge decreases slightly with increasing the discharge current, and the discharge voltage at fixed discharge current increases with increasing the separation electrode distance d.

The slight decrease of the discharge voltage (sustain voltage) with increasing discharge current might be explained by a slight increase of the gas temperature, which leads to a decrease of the gas density (at constant gas pressure) and thus decreases the resistance of the discharge region. At a more significant electrode gap separation (for $d > 12$mm.), the discharge channel started from the cathode surface had a filamentary shape that could not research the electrolyte's anode surface, which showed some type of corona discharge.
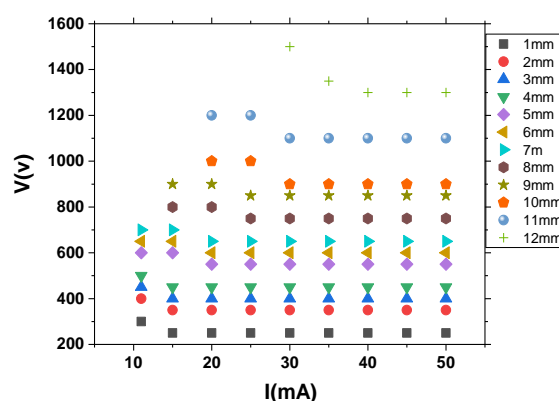

Figure 5: Current-voltage characteristics for plasma discharge in contact with liquid at several electrode spacings

3.2.3. Spectroscopic Characterization

Optical emission spectroscopy is acquired and carefully examined as a diagnostic tool for characterizing plasma in and in contact with liquid. We used spectrometers to cover a range of wavelengths between approximately 340 and 1000 nm, i.e., from ultraviolet to near-infrared range. The emission spectra shown in the current work were measured for electrode separation distance d of 3mm and discharge current of 30mA.

3.2.3.1. *Ultraviolet range*

Figure 6 shows the optical emission spectra in the range of 350–400 nm measured in the active region of the discharge (the whole region of the discharge).

The most intense emissions detected between 350 and 400 nm can be ascribed to the N_2 Second Positive System (SPS: $N_2[C^3\Pi_u] \rightarrow N_2[B^3\Pi_g]$) emission bands, with a dominant emission band assigned as (1,2) band (band head at 353.6 nm), (0,1) band (band head at 357.6nm), (1,3) band(band head at 375.5 nm), (0,2) band (band head at 380.4 nm) and (1,4) band (band head at 399.8 nm). The low emission at 391.4 nm is attributed to the (0-0) transition of the N_2 First Negative System (FNS: $N_2[B^3\Pi_g] \rightarrow N_2^+[A^3\Sigma^+_u]$). The spectrum of the N_2 Second Positive System in the UV range was typically accompanied by the N_2 First

_____

Negative System (FNS: $N_2[B^3\Pi_g] \rightarrow N_2^+ [A^3\Sigma^+_u]$) indicating the formation of $N_2 [A^3\Sigma^+_u]$ states. These long-lived metastable (energy~6 eV) are important as reservoirs of energy promoting plasma chemical reactions leading to condensed products in cleaning applications [22].
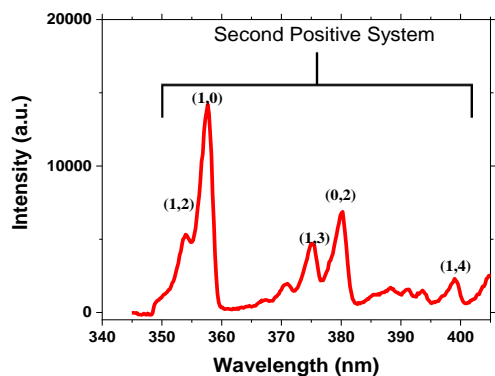

Figure 6: Emission spectra of DC discharge in the UV region
Gap: 3 mm; I= 30 mA

3.2.3.2. *Visible spectrum*

The visible spectrum recorded between 400 and 700 nm is shown in figure 7.

The N_2 Second Positive System (SPS: $N_2[C^3\Pi_u] \rightarrow N_2[B^3\Pi_g]$) emission (0,3) band head at 405.9 nm and (1-5) band at 426.97 nm. FNS (0-1) transition emitting at 427.8 nm is present. FeI transition *(3d^7(^4P)4s \rightarrow 3d^7(^4P)4p)* at 415.6 nm, Fe I transition ($3d^6(5D)4s^4p(3P°) \rightarrow 3d^6(5D)4s (6D)5s$) at 419.14 nm, Balmer H_β transition (2s 2S 1/2 $\rightarrow$ 4p2P°1/2) at 486.135 nm and H_a transition 2p-3d at 656.3 nm. In addition, to NaI atomic line at 589 nm was observed. Several emission lines of argon were also observed. The observed lines are presented in Table 1 with their transition parameters, which are referred to from the NIST database [23].
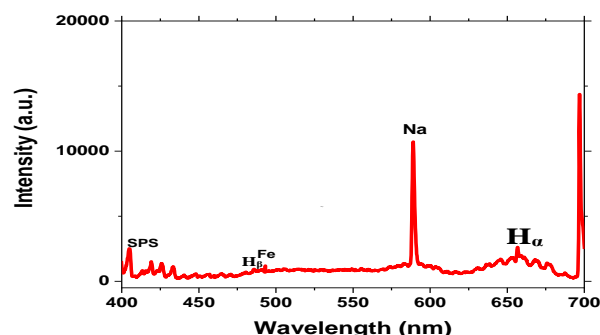

Figure 7: Emission spectra of DC discharge in the visible region
Gap: 3 mm; I= 30 mA.

3.2.3.3. *Near IR*

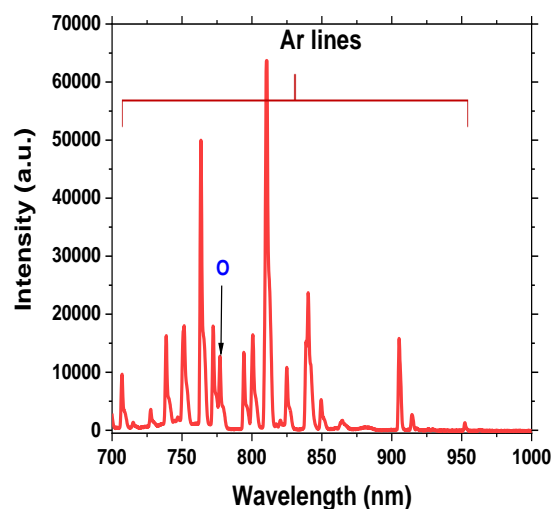Figure 8 shows the emission spectrum in the near Infrared region range from 700 and 1000 nm.

Figure 8: Emission spectra of DC discharge in the Near IR region
Gap: 3 mm; I= 30 mA.

Atomic oxygen line O I (transition $3p^5P$ $3s^5S^0$) at 777.41 nm and O I atomic line (transition 3p3P $3s^3S^0$) at 844.6 nm were observed in addition to several Ar atomic lines which are presented in Table 1[23].

3.2.4. *Discharge Temperatures*

The temperature of heavy species (neutrals and ions) belongs to the most critical discharge parameters. One of the usual techniques is UV-VIS emission spectroscopy, whenever the discharge emits light. Here, air entrained in the discharge region was used in most of the experiments. Thus, the major and the most radiative species in the UV-VIS region were N_2 molecules species. Consequently, the bulk gas temperature was determined by the rotational temperature of N_2, which is in equilibrium with the translational temperature of the gas. The rotational temperature of excited N_2 molecules was determined by comparing experimental spectra with simulated ones. It concerns the second positive system of N_2. We used software developed at the Technical University of Eindhoven to determine the rotational (T_{rot}) and vibrational (T_{vib}) temperatures of the discharge [14]-[24]. Figure 9 shows an experimental spectrum of N_2 second positive system $N_2[B^3\Pi_g]$ bands emitted from the discharge shown in Fig.6 together with the simulated spectrum.
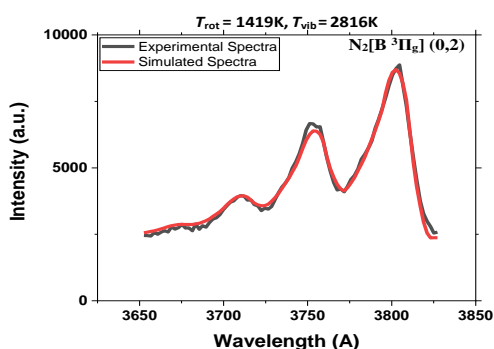
_____

Figure 9: Measured spectra and corresponding best fit modelled spectra

The best fits of T_{rot} and T_{vib} temperatures were 1419K and 2816K, respectively, with a correlation of 0.9956. The values of T_{rot} and T_{vib} indicate that the discharge was strongly non-equilibrium. Therefore, this kind of discharge is suitable for electrochemical applications because of the presence of energetic electrons, as can be seen in the following section. By using the current setup, we succeeded in synthesizing magnetic nanoparticles where this work will be published in forthcoming article.

3.3. *Chemical* Processes

Plasma electrochemistry is a highly reactive condition. Neutral gas is decomposed into a chemical mixture of ions, electrons, molecular, atomic radicals, excited metastable, and photons, as shown in figure 10. Electrochemical reactions can be driven by these species and secondary species formed at the vapor interface and in solution. The properties of free radicals produced in the plasma are essential.
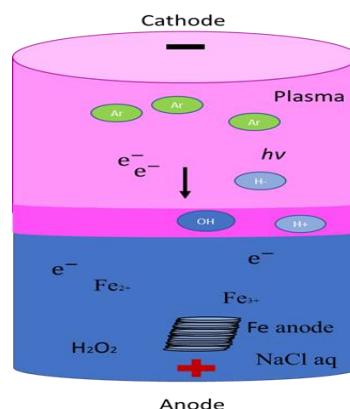

Figure 10: The chemical processes in plasma electrochemistry produced in contact with liquid

Table 1: The most powerful Ar atomic and ionic lines detected are listed below [23]

Line		λ (nm)	Upper state (i)	Low state(j)	A_{ij} (10^8 s^{-1})
Ar	I	415.859	5p	4s	0.0140
Ar	I	416.418	5p	4s	0.00288
Ar	I	418.188	5p	4s	0.00561
Ar	I	419.071	5p	4s	0.00280
Ar	I	419.832	5p	4s	0.0257
Ar	I	420.068	5p	4s	0.00967
Ar	I	425.936	5p	4s	0.0398
Ar	I	427.217	5p	4s	0.00797
Ar	I	452.232	5p	4s	0.000898
Ar	I	706.722	4p	4s	0.0380
Ar	I	714.704	4p	4s	0.00625
Ar	I	727.294	4p	4s	0.0183
Ar	I	738.398	4p	4s	0.0847
Ar	I	750.387	4p	4s	0.445
Ar	I	751.465	4p	4s	0.402
Ar	I	763.511	4p	4s	0.245
Ar	I	794.818	4p	4s	0.186
Ar	I	800.616	4p	4s	0.0490
Ar	I	801.479	4p	4s	0.0928
Ar	I	810.369	4p	4s	0.250
Ar	I	811.531	4p	4s	0.331
Ar	I	826.452	4P	4s	0.15
Ar	I	840.821	4p	4s	0.22
Ar	I	842.465	4p	4s	0.22
Ar	I	852.144	4p	4s	0.14
Ar	I	866.794	4p	4s	0.24
Ar	I	912.297	4p	4s	0.19
Ar	I	922.450	4p	4s	0.50
Ar	I	935.422	4P	4s	0.11
Ar	I	965.779	4p	4s	0.54

In the current work, there are conditions where the liquid itself serves as a conductive element in a direct current (DC) plasma circuit. One electrode is immersed, and the other is pendent over the solution, rather than being immersed. When applying a high voltage between the electrodes (in the kV order), the gas between the liquid and the pendent electrode breaks down to form a conductive discharge column. There are plenty of explanations for [25-30] specifying a general mechanism that occurs. Figure 10 shows the Ar plasma which generated over the aqueous solution of NaCl. An inert metal spiral such as Fe is submerged in the solution to direct the circuit. There are liquified metal ions Fe_2^+ in the solution. The chemistry can be extracted as

$$Fe_2^+ + 2e^- \rightarrow Fe \qquad (1)$$
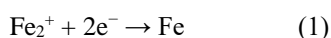
Still, the electrons delivered by the plasma can arise in highly different pathways. In the aqueous solution (NaCl), water molecules will be decomposed into OH radicals, and atomic hydrogen which can be combined to form H_2. In addition to the direct combination of OH radicals, H_2O_2 can be formed in many ways [31]. Dissociative electron attachment can indicate the formation of (H^-) which is a very strong species and can be melted into the liquid.

$$H_2O + e^- \rightarrow H^- + OH \qquad (2)$$

UV photons can be used as the energy source for generating atomic H and OH.

$$H_2O + hv \rightarrow H + OH \qquad (3)$$

Free electrons from the plasma and secondary electrons from ion radioactivity on the liquid surface have extensively strong reducing abilities due to their excessive energies; they can reduce virtually any metal ion in its liquefied form or most metal ions in the aqueous solution.

4. Conclusions

The formation of stable DC glow discharge generated between a needle cathode with electrolytic anode was investigated. NaCl solution was used as the electrolyte anode. The discharges were characterized by measuring the conception voltage in addition to discharge voltage and discharge current measurements. The measured discharge voltage and discharge current revealed that the discharge was working in glow mode. Measurement of rotational and vibrational temperatures in the discharge showed that the discharge was strongly nonequilibrium. The nonequilibrium state of the discharge in the current work is strong evidence to use the current experimental setup in electrochemical applications such as plasma assist electrolysis applications.

5. Acknowledgements

6. References

[1] Hajime Sakakitaa, Tetsuji Shimizu, and Satoru Kiyama, et al. Electrical characteristics of a low-temperature, atmospheric-pressure helium plasma jet, AIP Advances 11, 015323, (2021).
[2] Sing Wei Ng, et al. Characterization of an atmospheric pressure air plasma device under different modes of operation and their impact on the liquid chemistry, Journal of Applied Physics 129, 123303, (2021).
[3] Peter J. Bruggeman, et al. Plasma-driven solution electrolysis, J. Appl. Phys. 129, 200902, (2021).
[4] Chen, Z., Xu, R.-G., Chen, P., & Wang, Q. Potential Agricultural and Biomedical Applications of Cold Atmospheric Plasma-Activated Liquids with Self-Organized Patterns Formed at the Interface. IEEE Transactions on Plasma Science, 1–17, (2020).
[5] Levko, D., Arslanbekov, R. R., & Kolobov, V. I. Modified Paschen curves for pulsed breakdown. Physics of Plasmas, 26(6), 064502, (2019).
[6] G. Nayak, et al. Characterization of an RF-driven argon plasma at atmospheric pressure using broadband absorption and optical emission spectroscopy, Journal of Applied Physics 128, 243302, (2020).
[7] Sasaki, K., Nishiyama, S., & Shirai, N. Observation of 1 D −1 S forbidden optical emission of atomic oxygen in atmospheric-pressure N_2/O_2 plasma jet. Contributions to Plasma Physics, e202000061.(2020).
[8] Hodásová, Ľudmila, et al. Atmospheric pressure plasma liquid assisted deposition of polydopamine/acrylate copolymer on zirconia (Y-TZP) ceramics: a biocompatible and adherent nanofilm. RSC Advances, vol. 11, issue 28, pp. 17360-17368, (2021).
[9] Fiebrandt, M., Bibinov, N., & Awakowicz, P. Determination of atomic oxygen state densities in a double inductively coupled plasma using optical emission and absorption spectroscopy and probe measurements. Plasma Sources Science and Technology, (2020).
[10] J Liu, N Shirai, K Sasaki. Synthesis mechanism of cuprous oxide nanoparticles by atmospheric-pressure plasma electrolysis, Journal of Physics D: Applied Physics 54 (10), 105201, (2021).
[11] Zheng, Y., Wang, L., & Bruggeman, P. Modeling of an atmospheric pressure plasma-liquid anodic interface: Solvated electrons and silver reduction. Journal of Vacuum Science & Technology A, 38(6), 063005, (2020).

_____

[12] Mohamed H, Clemen R, Freund E, Lackmann J-W, Wende K, Connors J, et al. non-thermal plasma modulates cellular markers associated with immunogenicity in a model of latent HIV-1 infection. PLoS ONE 16(3): e0247125, (2021).

[13] Mohamed H, G Nayak, N Rendine, B Wigdahl, FC Krebs, PJ Bruggeman, Vandana Miller, Non-Thermal Plasma as a Novel Strategy for Treating or Preventing Viral Infection and Associated Disease, Frontiers in Physics 9, 286, (2021).

[14] Nasser N. Morgan and Mansour ElSabbagh, Plasma Chem Plasma Process, 37, 1375, (2017).

[15] Shirai, N., Ichinose, K., Uchida, S., & Tochikubo, F. Influence of liquid temperature on the characteristics of an atmospheric dc glow discharge using a liquid electrode with a miniature helium flow. Plasma Sources Science and Technology, 20(3), 034013. (2011).

[16] Paschen, F, Ueber die zum Funkenübergang in Luft, Wasserstoff und Kohlensäure bei verschiedenen Drucken erforderliche Potentialdifferenz. Annalen Der Physik, 273(5), 69–96, (1889).

[17] Dengming Xiao, Gas Discharge and Gas Insulation, Springer-Verlag Berlin Heidelberg, (2016).

[18] Bakhtier Farouk, David Staack, Tanvir Farouk, Alexander Gutsol, Alexander Fridman Proceedings of the International Conference on Mechanical Engineering 2007, (ICME2007) 29-31 December 2007, Dhaka, Bangladesh. (2007).

[19] Lieberman, Michael A.; Lichtenberg, Allan J, Principles of plasma discharges and materials processing (2nd ed.). Hoboken, N.J.: Wiley-Interscience. 546, (2005).

[20] Rathore, K., Wakim, D., Chitre, A., & Staack, D, Glow discharge characteristics of non-thermal microplasmas at above atmospheric pressure. Plasma Sources Science and Technology, (2020).

[21] D. Staack, B. Farouk, A. Gutsol, et al., "Characterization of a dc atmospheric pressure normal glow discharge," Plasma Sources Science & Technology, vol. 14, no. 4, pp. 700-711, (2005).

[22] Fridman A and Kennedy L A, Plasma Physics and Engineering (New York: Taylor and Francis), (2004).

[23] NIST. NIST Atomic Spectra Database. Accessed:[Online].physics.NIST.gov/PhysRefData/ASD/lines_form.HTML.

[24] Aldea E Private communications.

[25] Koo I G, Lee M S, Shim J H, Ahn J H and Lee W M,J. Mater. Chem. 15 4125, (2005).

[26] [26] Baba K, Kaneko T and Hatakeyama R, Appl. Phys.Express 2 5006, (2009).

[27] El Abedin S Z, Pölleth M, Meiss S, Janek J and Endres F, Green Chem. 9 549, (2007).

[28] Saito N, Hieda J and Takai O, Thin Solid Films 518 912, (2009).

[29] Acayanka E, Djowe A T, Laminsi S, Tchoumkwé C, Nzali S, Mbouopda A P, Ndifon P and Gaigneaux E, Plasma Chem. Plasma Process. 33 1, (2013).

[30] Harris DC, Quantitative Chemical Analysis, New York: Macmillan, (2015).

[31] Lofrano, G.; Pedrazzani, R.; Libralato, G.; Carotenuto, M. Advanced Oxidation Processes for Antibiotics Removal: A Review. Curr. Org. Chem, 21, 1–14, (2017).

_____